Wide-angle coupling into rod-type photonic crystals with ultralow reflectance

L. C. Botten,[1,*] T. P. White,[2] C. Martijn de Sterke,[2] and R. C. McPhedran[2]
[1]*Centre for Ultrahigh-Bandwidth Devices for Optical Systems (CUDOS) and Department of Mathematical Sciences, University of Technology, Sydney, Broadway NSW 2007, Australia*
[2]*CUDOS and School of Physics,University of Sydney, NSW 2006, Australia*
(Received 5 December 2005; published 10 August 2006)

We describe the surprising phenomenon of near-perfect coupling from free space into uniform two-dimensional rod-type photonic crystals over a wide range of incident angles. This behavior is shown to be a generic feature of many rod-type photonic crystal structures that is related to strong forward scattering resonances of the individual cylinders. We explain these results using both semianalytic analysis and two-dimensional numerical calculations and identify the conditions under which efficient, wide-angle coupling can occur. The results may lead to more efficient designs for in-band photonic crystal devices such as superprisms and self-collimation based photonic circuits.

DOI: 10.1103/PhysRevE.74.026603 PACS number(s): 42.70.Qs, 42.25.Bs, 42.25.Fx, 42.79.Dj

I. INTRODUCTION

Photonic crystals (PCs) are one of the most versatile structures being considered as a platform for future integrated optical chips. When operating at frequencies within a photonic band gap, two-dimensional (2D) PCs can be used for wave guiding, resonant structures, lasers, filters, and a range of other operations. Alternatively, when light is coupled into propagating Bloch modes of the PC, the periodic structure can exhibit unique dispersion characteristics. In this case, one can access a range of other interesting properties such as superprism effects, negative refraction, perfect lensing, and autocollimation. To use these effects in practical devices it is essential that light can be coupled efficiently into and out of the PC structure with minimal backreflection. This is necessary not only to keep the insertion losses low, but also to prevent light from being scattered into other parts of a device where it may cause interference and crosstalk. The latter issue will be especially important in compact integrated optical circuits consisting of many components on a single chip.

While one of the main attractions of PC devices is their compactness, this also presents many practical challenges when interfacing these PC components to conventional optical systems. Several efficient methods have been developed for coupling to waveguide-based devices [1–4], but the challenge remains to find a practical solution for coupling light into the extended Bloch modes of a uniform PC lattice for in-band applications. The main approaches proposed in the literature for improving coupling to air-hole type PCs involve modifications to the front and rear interfaces of the structure. One such method is analogous to conventional thin-film coatings whereby the first few layers of cylinders are tuned to enhance the transmission properties via resonant coupling. This approach tends to result in narrow bandwidth transmission [5], although the bandwidth can be improved with multilayered gratings [6]. A second approach is to change the size and/or shape of the air holes to modify gradually the field profile as it approaches the PC slab, effectively creating an apodized interface [5,7]. An alternative method proposed by Witzens *et al.* [8], that does not require interface modifications, is to place a waveguide above a PC slab and use evanescent coupling to transfer light from the waveguide into counterpropagating Bloch modes of the PC.

Here we study the transmission properties of rod-type PCs and demonstrate that it is possible to couple more than 99% of incident light into such structures over a wide range of incident angles. In contrast to hole-type PCs, this can be achieved without making any modifications to the interface. The geometry we consider is shown in Fig. 1: a plane wave is incident from free space at an angle ϕ_0 onto a semi-infinite 2D PC consisting of dielectric rods of refractive index $\nu = \nu_c$, embedded in air ($\nu=1$). This is a generic problem that is relevant to almost all applications in which light must be coupled into the Bloch modes of a uniform PC.

We recently reported the optimization of a PC to exhibit both highly efficient coupling and self-collimation properties [9] for angles of incidence $-22.5° \leqslant \phi_0 \leqslant 22.5°$. This was achieved in a rod-type PC slab geometry without modification to the interface of the PC. In this paper we investigate the underlying physics that determines the coupling properties of rod-type PCs and identify the conditions under which efficient coupling occurs. The remainder of this paper consists of five sections. In Sec. II, we present numerical results for plane wave transmission into semi-infinite 2D rod-type PCs as in Fig. 1 and demonstrate highly efficient coupling for a wide range of incident angles. In Sec. III we show that

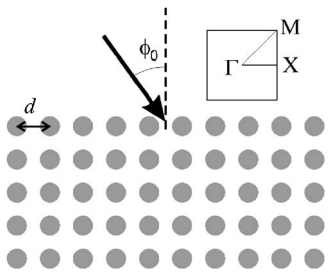

FIG. 1. Geometry used to calculate the transmission of a plane wave incident on a semi-infinite PC at an angle ϕ_0.

*Electronic address: lindsay.botten@uts.edu.au

the high transmission features coincide with forward scattering resonances of the individual cylinders, and show that this leads to a simple physical interpretation of the PC transmission results. A rigorous analysis of this relationship is presented in Secs. IV and V via the properties of a one-dimensional (1D) infinite array of cylinders, i.e., a grating. In Sec. IV we derive a semianalytic result showing that near-perfect coupling occurs when each constituent grating layer of the PC scatters all incident light into a single forward-propagating grating order. We next present in Sec. V an analysis of the grating properties and show that nulls in the grating reflectance spectrum occur close to the forward scattering resonances of the individual cylinders. We conclude with the identification of two conditions for near-perfect coupling: first, the incident light must be mostly forward scattered by each of the cylinders, and second, each grating layer forming the PC lattice must scatter light into only a single propagating grating order.

II. PLANE WAVE TRANSMISSION PROPERTIES

In this section we consider the geometry shown in Fig. 1 in which a plane wave is incident at an angle ϕ_0 onto a semi-infinite 2D PC. The reflection of the incident field is described by the matrix $\mathbf{R}_\infty$, defined as the reflection scattering matrix for a plane wave incident from free space onto a semi-infinite PC. In this notation, the (i,j)th element of $\mathbf{R}_\infty$ is the complex amplitude for reflection into grating order i for a plane wave incident in order j with unit power. Here, we calculate $\mathbf{R}_\infty$ using a Bloch mode scattering matrix method [10,11] (BMM), which yields the reflection into both propagating and evanescent grating orders. Since we are interested in the reflected power, and no energy is carried away from the PC interface by the evanescent states, $\mathbf{R}_\infty$ is truncated to contain only those elements corresponding to propagating plane wave orders. Thus, when only a single reflected order is supported, $\mathbf{R}_\infty$ can be treated as a scalar and the total reflected power is $\varepsilon_R=|\mathbf{R}_\infty|^2$. When multiple reflected orders are present, the total reflectance is calculated as a sum over the reflectance into each order. For the purely 2D structures composed of lossless dielectrics considered here, there are no additional loss mechanisms so the transmitted power is simply $\varepsilon_T=1-\varepsilon_R$.

The BMM is a powerful tool for understanding single interface properties as it allows semi-infinite structures to be studied without the need for absorbing boundary conditions. Thus, the interface reflection effects can be isolated from the coherent reflection effects observed in structures with a finite number of PC layers. The BMM also provides a rigorous mathematical framework for studying how each component of the PC contributes to the properties of the bulk structure. In the BMM formulation, the bulk PC properties are calculated from the scattering properties of the individual grating layers which, in turn, are derived using a multipole method that implicitly includes the scattering characteristics of the individual cylinders. This systematic breakdown of the structure into basic components is used in Secs. IV and V to explain the origin of the highly efficient transmission illustrated in Fig. 2.

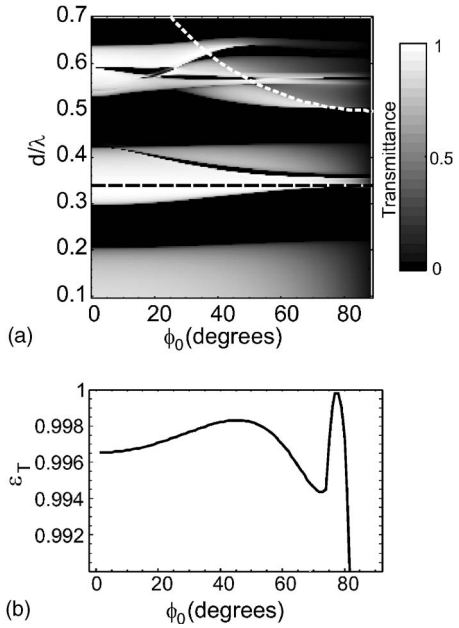

FIG. 2. (a) Transmittance ε_T vs dimensionless frequency d/λ and incident angle ϕ_0 for the 2D PC described in the text. The dashed white line indicates the maximum frequency for which the single diffracted grating order condition is satisfied, as discussed in Sec. V. (b) Transmittance vs ϕ_0 at $d/\lambda=0.34$, indicated by the dashed black line in (a).

Figure 2(a) shows the transmittance of an incident plane wave as a function of ϕ_0 and normalized frequency d/λ for a square lattice PC of rods with $\nu_c=3.0$ and $r_c=0.34d$. The light is polarized with the electric field parallel to the cylinders (TM). The striking feature in this figure is the white high transmission "finger" crossing the diagram at a dimensionless frequency of approximately $d/\lambda=0.34$ lying in the second band. At this frequency, indicated by the black dashed line in Fig. 2(a), the transmittance into the PC exceeds 99.4% for incident angles from 0° to 80°, as shown in Fig. 2(b). The third band also exhibits a high transmission region ($\varepsilon_T>99.5\%$), indicated by the white band near $d/\lambda=0.58$, although this only extends to incident angles of about 30°. We also note that the transmittance into the first band, although relatively high for normal incidence, does not exceed 90%.

Similar features to those shown in Fig. 2 occur in a wide range of rod-type PC structures, for both TE (magnetic field parallel to cylinders) and TM (electric field parallel to cylinders) polarizations and for both square and triangular lattices. To illustrate the generic nature of the high transmission features, Fig. 3 shows the maximum acceptance angle ϕ_{max} plotted as a function of the cylinder radius for three different transmittance levels. Here ϕ_{max} is defined for a transmittance T_{min} such that $T>T_{min}$ for all angles in the range $0\leqslant|\phi_0|\leqslant\phi_{max}$. In the range $0.32<r_c/d<0.4$, more than 99% of the incident light is transmitted into the PC for all incident angles up to 60°. We also find that the peaks in the transmission spectrum depend only weakly on the lattice period and incident angle and are almost identical for square and triangular lattices formed from the same rods. These last three

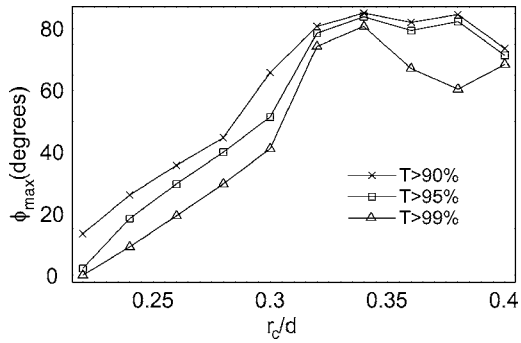

FIG. 3. Maximum acceptance angle ϕ_{max} plotted as a function of normalized cylinder radius for a square lattice of rods of index $\nu_c=3.0$ in air. The three curves correspond to minimum transmittance levels of 90%, 95%, and 99% for an incident plane wave of TM polarization.

observations imply that the near-perfect transmission features observed in Fig. 2 result from a property of the individual rods rather than the bulk lattice.

While in the remainder of this paper we present numerical results for the PC considered in Fig. 2, the analysis is generally applicable. We show in the following sections that the high-transmission properties originate from the individual scattering characteristics of the high-index rods, which influence the properties of a layer of cylinders, and in turn the properties of the 2D lattice of rods. In Sec. III, we discuss the relevant scattering properties of a single dielectric cylinder: the scattering cross section and the asymmetry parameter.

III. SINGLE CYLINDER SCATTERING

Although photonic crystals rely intrinsically on coherent scattering for many of their unique properties, the individual scattering elements contribute to the detailed characteristics of the structure. Economou [12] and Soukoulis [13] showed a correspondence between the bandgaps in three-dimensional (3D) PCs formed from dielectric spheres and the Mie resonances of the spheres and similar results have been shown for 2D PCs consisting of dielectric cylinders [14]. The relationship between scattering resonances and PC transmittance properties is not so well understood. Gantzounis *et al.* [15] recently related Mie resonances to resonant reflection and transmission in 3D PCs of polaritonic spheres, but only presented results for normal incidence. Here we consider 2D PCs of dielectric cylinders and show that there is not only a correspondence between cylinder resonances and band position, but also a direct relationship between forward scattering and the transmittance of plane waves incident on a PC. Although the results presented here are strictly 2D, 3D finite difference time domain (FDTD) calculations indicate that the characteristic high transmission features are also exhibited in realistic PC slab structures consisting of finite length rods [9].

The scattering properties of an infinite dielectric cylinder are well understood and can be calculated for nonconical incidence following the method of van de Hulst [16]. While the treatment presented here is identical to that in Ref. [16], the notation is modified in order to maintain consistency with the multipole analysis in Sec. V. Results are presented for TM polarization but similar scattering behavior also occurs for TE polarization.

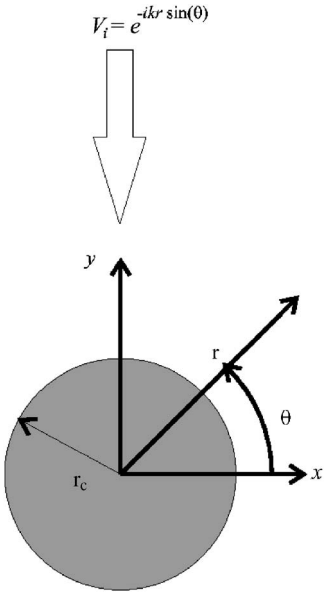

FIG. 4. Single cylinder scattering geometry: plane wave incident from above is scattered in directions θ, where $\theta=-\pi/2$ corresponds to forward scattering.

Consider first the geometry illustrated in Fig. 4 in which a plane wave of TM polarization is incident on a cylinder of radius a and refractive index ν_c in air. Note that in this geometry, $\theta=\pi/2(-\pi/2)$ corresponds to backward (forward) scattering. The electric field $[E_z=V(\boldsymbol{r})\exp(-i\omega t)]$ external to the cylinder is expanded in a basis of cylindrical harmonic functions

$$V(\boldsymbol{r}) = \sum_{n=-\infty}^{\infty} [a_n J_n(kr) + b_n H_n^{(1)}(kr)] e^{in\theta}, \tag{1}$$

where $(r,\theta)=(x,y)$, with $x=r\cos\theta$ and $y=r\sin\theta$. The scattered field is associated with the b_n coefficients and the incident field with the a_n coefficients. The incident plane wave field can be written as

$$V_i = e^{-ikr\sin\theta} \tag{2}$$

$$= \sum_n a_n J_n(kr) e^{in\theta}, \quad \text{where } a_n = (-1)^n. \tag{3}$$

Using the standard approach for deriving the outgoing field coefficients b_n, the tangential field components are matched on the cylinder boundary, which imposes the condition [16,17]

$$b_n = R_n a_n, \quad \text{where } R_n = -\frac{1}{1+iM_n} \tag{4}$$

and

$$M_n = \frac{\nu_c J_n'(k\nu_c r_c) Y_n(kr_c) - J_m(k\nu_c r_c) Y_m'(kr_c)}{\nu_c J_n'(k\nu_c r_c) J_n(kr_c) - J_m(k\nu_c r_c) J_m'(kr_c)}, \tag{5}$$

for TM polarization.

Here we are most interested in the far-field form of the scattered field that follows from the large-argument asymptotics of the Hankel functions [18], and which leads to

$$V_s(\boldsymbol{r}) = \sum_n b_n H_n^{(1)}(kr) e^{in\theta} \tag{6}$$

$$\approx \sqrt{\frac{2}{\pi kr}} e^{i(kr-\pi/4)} T_c(\theta), \tag{7}$$

where

$$T_c(\theta) = \sum_n b_n e^{in(\theta-\pi/2)}. \tag{8}$$

Two scattering parameters relevant to this discussion are the scattering cross section per unit length of the cylinder

$$c_{\text{scat}} = \frac{2}{\pi k} \int_{-\pi}^{\pi} |T_c(\theta)|^2 d\theta = \frac{4}{k} \sum_{n=-\infty}^{\infty} |b_n|^2, \tag{9}$$

and the asymmetry parameter, defined as the weighted average of $-\sin(\theta)$ with respect to the scattering amplitude

$$g = -\langle \sin(\theta) \rangle = -\frac{\int_{-\pi}^{\pi} |T_c(\theta)|^2 \sin(\theta) d\theta}{\int_{-\pi}^{\pi} |T_c(\theta)|^2 d\theta}. \tag{10}$$

Here, $|g|<1$ and $g>0$ ($g<0$) corresponds to dominant forward (backward) scattering.

Figure 5(a) shows the normal incidence transmittance spectrum for the square PC lattice considered in Fig. 2. The curves in Figs. 5(b) and 5(c) show the scattering cross section and asymmetry parameter, respectively, as functions of r_c/λ for a single cylinder of index $\nu_c=3.0$ in air. In both plots, the solid curve is calculated for a multipole truncation order of $N_m=3$, where Eq. (8) is summed over $n=-N_m, -N_m+1, \ldots, N_m$. The remaining curves correspond to truncation orders of $N_m=0,1,2$. Observe that the single monopole term ($N_m=0$) describes accurately the single cylinder properties for frequencies up to the first band of the PC, while the dipole approximation ($N_m=1$) is sufficient for the second band. While additional multipole terms are required in the field expansion for higher frequencies, the $N_m=3$ curves in Figs. 5(b) and 5(c) have converged to graphical accuracy for the plotted frequency range. The relative importance of each multipole order can also be inferred from Fig. 5(d) which shows the amplitudes of the first four multipole coefficients $|b_n|$. In Sec. V we use the dipole approximation to derive a semianalytic result relating the single cylinder scattering resonances to the transmission of a grating.

Figures 5(a) and 5(b) show a clear correspondence between the band position (indicated by nonzero transmittance) and peaks in c_{scat}, as has been observed by others [13,14]. This does not explain, however, why the transmittance into the second and third bands exceeds 99%, whereas transmittance into the first band is less than 90%. To understand this feature, it is necessary to consider the direction of the scattered fields, as measured by the asymmetry parameter in Fig.

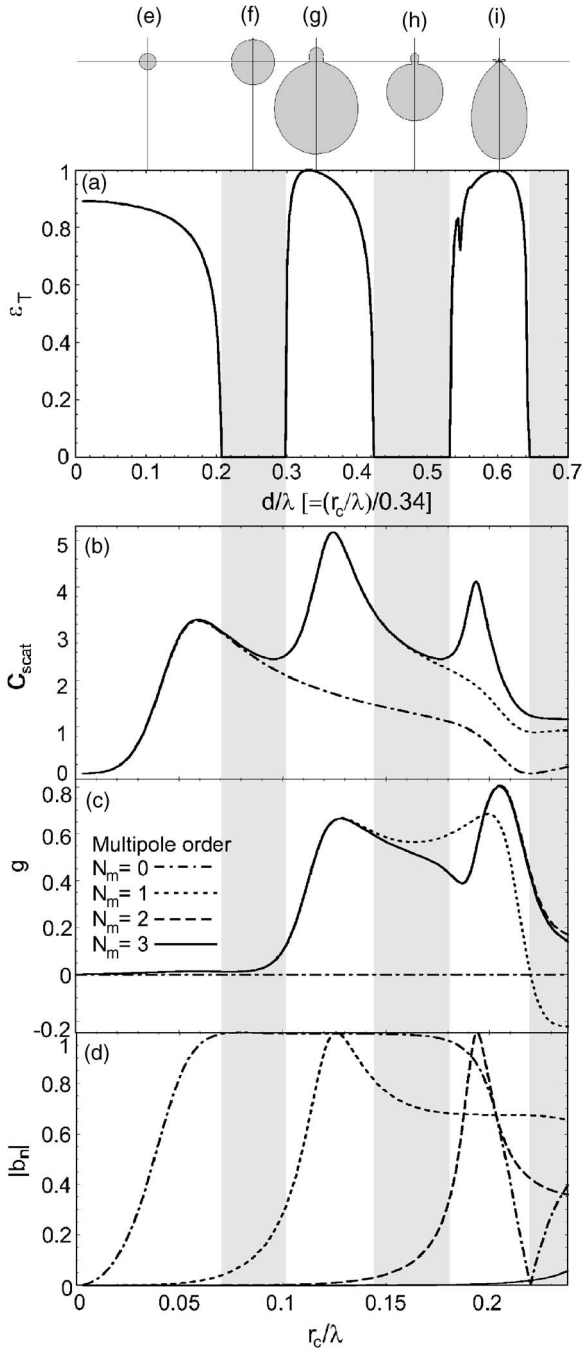

FIG. 5. (a) Normal incidence transmittance for the PC lattice considered in Fig. 2. (b), (c) Single cylinder scattering cross section and asymmetry parameter, respectively, plotted as a function of r_c/λ for the same frequency range as (a). Both parameters are calculated for multipole truncation orders $N_m=0,1,2,3$, where the $N_m=3$ curve (solid) is converged to within graphical accuracy. (d) Multipole scattering coefficients $|b_n|$ plotted for $n=0-3$. Shaded regions in (a)–(d) indicate the band gaps of the bulk PC. (e)–(i) Scattering patterns given by $|T(\theta)|^2/k$ for $r_c/\lambda=0.034$, 0.085, 0.116, 0.163, and 0.204 for light incident from above.

5(c) and the scattering patterns (e)–(i), plotted for frequencies in the first band, the first gap, the second band, the second gap, and the third band, respectively. The scattering patterns are polar plots of $|T_c(\theta)|^2/k$, such that the area enclosed by each diagram is proportional to c_{scat}. In the second and third bands, where the transmittance is highest, the peak in c_{scat} coincides approximately with a peak in g, indicating a forward scattering resonance. In the first band g remains positive but approaches zero, despite there being a small, broad peak in c_{scat}. Thus, although there is still significant scattering from each cylinder at low frequencies, the scattering direction is almost isotropic, with Eqs. (7)–(9) being dominated by the b_0 term as discussed above. This can also be observed in the scattering patterns in Figs. 5(e) and 5(f). As the frequency is increased, higher-order scattering terms become significant and can result in strong directional scattering. For example, the c_{scat} peaks near $d/\lambda=0.36(r_c/\lambda=0.112)$ and $d/\lambda=0.60(r_c/\lambda=0.204)$ correspond to maxima in b_1 and b_2, respectively, as seen in Fig. 5(d). Each of these resonances results in strong forward scattering as indicated by the g curve of Fig. 5(c) and the scattering patterns in Figs. 5(g) and 5(i).

While the results plotted in Fig. 5 are not conclusive proof that scattering resonances of individual cylinders enhance the transmission into a PC, they provide a physically intuitive explanation for the results in Fig. 2. In the next two sections we provide a rigorous mathematical analysis that demonstrates first, the relationship between the transmission properties of a grating and those of a bulk PC, and second, the relationship between single cylinder resonances and grating transmission properties.

IV. RELATIONSHIP BETWEEN GRATING AND PC TRANSMISSION PROPERTIES

In this section we derive a semianalytic expression relating the plane wave reflection properties of a semi-infinite PC to the scattering of a plane wave from a single grating layer of cylinders. The analysis is valid in the long wavelength regime in which there is only a single propagating plane wave order in reflection and transmission. For a PC consisting of dielectric rods in free space, this corresponds to scaled frequencies of $d/\lambda<1/(1+|\sin(\phi_0)|)$. In Fig. 2, the single grating order condition is satisfied below the dashed white line, and so the treatment is valid for the first two bands at all incident angles, and the third band for $\phi_0\lesssim 50°$. In this regime, the reflectance of the bulk PC is determined largely by the reflectance of the constituent grating as can be seen in Fig. 6, which shows the normal incidence transmittance spectra for the bulk PC and a single grating layer. Observe that the perfect transmission features in the PC spectrum coincide exactly with those of the grating. Thus, the study of efficient coupling of light into a bulk PC can be reduced to the less complex grating problem.

Consider first the calculation of the plane wave scattering matrix $\mathbf{R}_\infty$, which characterizes the reflection of a plane wave incident on a semi-infinite PC from free space at an angle ϕ_0. Within the PC, each layer is treated as a 1D infinite grating of cylinders, and the fields between each layer are expressed

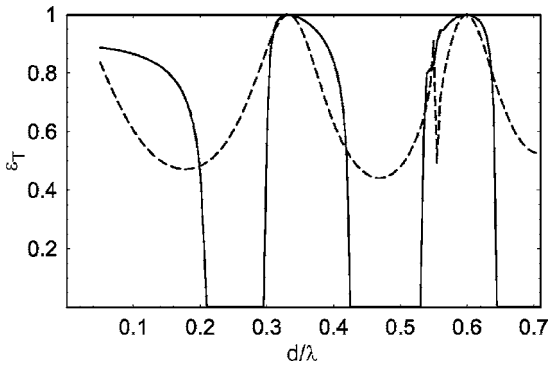

FIG. 6. Normal incidence grating (dashed curve) and PC (solid curve) transmittance spectra for the PC considered in Sec. II.

in terms of plane waves [10]. For a given grating in the PC, the fields above and below (denoted by $j=1$ and $j=2$, respectively) are expanded in the form

$$V^{(j)}(x,y)=\sum_{p=-\infty}^{\infty}\chi_p^{-1/2}[f_p^{(j)-}e^{-i\chi_p(y-y_j)}+f_p^{(j)+}e^{i\chi_p(y-y_j)}]e^{i\alpha_p x}, \tag{11}$$

where $k=2\pi/\lambda$, $\alpha_0=k\sin(\phi_0)$, $\alpha_p=\alpha_0+pK$, $\chi_p=\sqrt{k^2-\alpha_p^2}$, and $K=2\pi/d$. In the Bloch mode scattering matrix method [10] we may write $\mathbf{R}_\infty=\boldsymbol{\mathcal{F}}_+\boldsymbol{\mathcal{F}}_-^{-1}$, where $\boldsymbol{\mathcal{F}}_-$ and $\boldsymbol{\mathcal{F}}_+$ are matrices whose columns contain the forward ($\boldsymbol{f}^-$) and backward ($\boldsymbol{f}^+$) propagating parts of the plane wave representations of the Bloch modes of the bulk structure.

In the long wavelength regime that is of interest, there is only a single propagating plane wave and so the transmittance into the crystal is given by

$$\varepsilon_T=1-[R_{\infty(00)}]^2, \tag{12}$$

where the subscripted (00) refers to the specular order of diffraction for both reflected and transmitted waves. We now seek to relate the reflection properties of the bulk structure, encapsulated within $\mathbf{R}_\infty$, to the corresponding properties of the gratings that constitute the crystal. These are linked by the transfer matrix eigenvalue equation [19]

$$\boldsymbol{\mathcal{T}}\boldsymbol{f}=\mu\boldsymbol{f}, \tag{13}$$

where

$$\boldsymbol{\mathcal{T}}=\begin{pmatrix}\boldsymbol{T}-\boldsymbol{R}'\boldsymbol{T}'^{-1}\boldsymbol{R} & \boldsymbol{R}'\boldsymbol{T}'^{-1}\\ -\boldsymbol{T}'^{-1}\boldsymbol{R} & \boldsymbol{T}'^{-1}\end{pmatrix} \quad \text{and} \quad \boldsymbol{f}=\begin{pmatrix}\boldsymbol{f}_-\\ \boldsymbol{f}^+\end{pmatrix}, \tag{14}$$

with $\boldsymbol{R}$ and $\boldsymbol{T}$ denoting the reflection and transmission scattering matrices for a grating layer for incidence from above, and $\boldsymbol{R}'$ and $\boldsymbol{T}'$ being the corresponding quantities for incidence from below [19].

When the spatial frequency of the fields is sufficiently low, i.e., for sufficiently long wavelengths, the high frequency components of the field expansions can be removed and a scalar approximation (comprising only the single specular order) used in place of the rigorous solution. Proceeding formally with this assumption, we are led to an eigenvalue equation which appears as a quadratic equation

$$\mu^2 - 2b\mu + 1 = 0, \quad \text{where } b = \frac{T^2 - RR' + 1}{2T}. \tag{15}$$

Here, R and T refer to the specular order elements R_{00} and T_{00} of the respective grating scattering matrices. Note that in the scalar approximation, $T=T'$, by reciprocity. Furthermore, in a square lattice each grating layer must exhibit up-down symmetry such that $R=R'$. Accordingly, b may be reduced to $b=\cos(\arg T)/|T|$ for a lossless square lattice after observing that $|R|^2+|T|^2=1$ and $\arg T-\arg R=\pm\pi/2$. Note that in a passband of the PC, in which we expect complex μ of unit magnitude, $|b|<1$. Further manipulation of the transfer matrix equation (14) allows us to derive a quadratic equation in $R_\infty=f_+/f_-$, that links directly the reflection characteristics of the semi-infinite PC and the transmission and reflection properties of the grating, namely,

$$R_\infty^2 - 2cR_\infty + 1 = 0,$$

$$\text{where} \quad c = -\frac{T^2 - R^2 - 1}{2R} = \frac{\cos(\arg R)}{|R|}. \tag{16}$$

Here, b and c are functions of grating reflection and transmission only and are related to one another by

$$c^2 - 1 = \frac{|T|^2}{|R|^2}(1 - b^2). \tag{17}$$

Hence, we deduce that $c>1$ or $c<-1$ in a passband, yielding two real solutions for R_∞ that are reciprocals of one another, with the physical solution chosen according to $|R_\infty|<1$. It is straightforward to show that a low reflectance of the constituent grating, $|R|^2$, leads to a low reflectance of the bulk structure $|\mathbf{R}_\infty|^2$, with the two quantities related by

$$R_\infty \approx \frac{1}{2c} = \frac{|R|}{2\cos(\arg R)}. \tag{18}$$

Equation (18) is consistent with the results in Fig. 6, which clearly illustrates the coincidence of the near-zero reflectance features in the grating and the semi-infinite PC transmission spectra. Hence, our study of the highly efficient coupling shown in Fig. 2 is simplified to one of understanding perfect transmission of a plane wave through a 1D grating of cylinders. This is the subject of the next section in which we demonstrate that such spectral features are closely related to forward scattering resonances of the constituent cylinders.

V. RELATIONSHIP BETWEEN SINGLE-CYLINDER SCATTERING AND GRATING TRANSMISSION PROPERTIES

In this section we focus on the transmission properties of a grating composed of a 1D array of identical cylinders and show that the minimum reflectance occurs at frequencies close to the scattering resonances of the individual cylinders that form the grating. Moreover, we explain why this frequency does not change significantly with incident angle. When combined with the results of Sec. IV, the analysis provides a direct link between the cylinder scattering resonances and efficient coupling to the bulk PC lattice.

We begin by considering the multipole formulation for diffraction of a plane wave by a grating composed of cylinders of radius r_c, refractive index ν_c and period d. A plane wave field $\boldsymbol{\delta}$ incident from above at an angle ϕ_0 gives rise to plane wave fields above and below the grating composed of a superposition of propagating and evanescent grating orders. Similar to the single cylinder, the field in the vicinity of each cylinder is expanded in terms of cylindrical harmonics in the form of Eq. (1) where the b_n coefficients are again associated with the scattered field. The a_n coefficients are derived by observing that the regular part of the field in the vicinity of any cylinder is due to the outgoing field sourced on all other cylinders plus fields generated by exterior sources (which in this case is the incident plane wave). This leads to the matrix field identity [17]

$$\boldsymbol{a} = \boldsymbol{S}\boldsymbol{b} + \boldsymbol{J}^-\boldsymbol{\chi}^{-1/2}\boldsymbol{\delta} \tag{19}$$

in which $\boldsymbol{S}=[S_{lm}]=[S_{l-m}]$, with the S_n denoting the lattice sums

$$S_n = \sum_{s\neq 0} H_n^{(1)}(k|s|d)e^{-in\arg(s)}e^{i\alpha_0 sd} \tag{20}$$

that characterize the scattering contributions associated with a particular multipole order due to the entire grating. The matrix $\boldsymbol{J}^-=[J_{np}]$, where $J_{np}^-=(-1)^n\exp(-in\phi_p)$ and $\exp(i\phi_p)=(\chi_p+i\alpha_p)/k$, performs a coordinate transformation from the plane wave basis to the cylindrical harmonic basis. Here $\boldsymbol{\chi}^{-1/2}$ is a normalization term consisting of elements χ_p corresponding to the normal wave vector component of grating order p.

Combining Eqs. (4) and (19) we form an expression for the multipole source coefficients generated by the incoming field

$$\boldsymbol{b} = -(\boldsymbol{S}' + i\boldsymbol{M})^{-1}\boldsymbol{J}^-\boldsymbol{\chi}^{-1/2}\boldsymbol{\delta}, \tag{21}$$

where $\boldsymbol{S}'=\boldsymbol{S}+\boldsymbol{I}$, with $\boldsymbol{I}$ denoting the unit matrix. From this, the reflected and transmitted plane wave coefficients may be reconstructed (see Appendix A). We are interested in the long wavelength case, for which only a single plane wave order propagates. For simplicity we initially consider only normally incident light, in which case the reflection and transmission coefficients for the specular order are given by

$$r_0 = \frac{2}{d\chi_0^{1/2}}\sum_n b_n, \tag{22}$$

$$t_0 = 1 + \frac{2}{d\chi_0^{1/2}}\sum_n (-1)^n b_n, \tag{23}$$

noting that for this symmetric case $b_{-n}=b_n$. Thus the backward and forward scattered fields have respective amplitudes that are proportional to $b_0+2b_1+2b_2+\cdots$ and $b_0-2b_1+2b_2+\cdots$, where the expression may be satisfactorily truncated to a given multipole order that depends on the frequency of the light.

We now proceed to verify the empirical results of Sec. III that indicated a correspondence between forward scattering

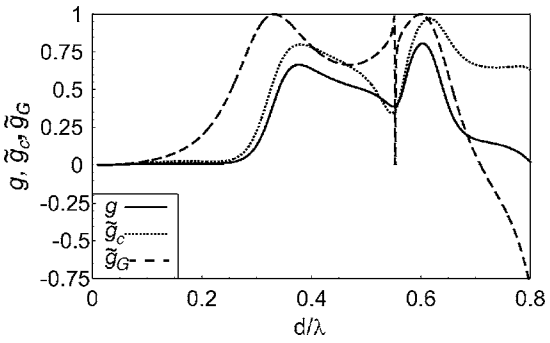

FIG. 7. Comparison of single cylinder scattering parameters g (solid) and $\tilde{g}_c$ (dashed) for a cylinder of index $\nu_c=3.0$ and radius $r_c=0.34d$, and $\tilde{g}_G$ (dotted) for a grating of period d formed from identical cylinders. The horizontal axis is expressed in units of the normalized grating frequency, d/λ.

by each cylinder and efficient transmission into the PC. To do this, we first return to the single cylinder scattering analysis of Sec. III, and derive an appropriate scattering parameter that allows direct numerical and analytic comparison between the grating and cylinder properties. Recall from Sec. III that we used the asymmetry parameter g (10) to identify strong forward scattering by a single cylinder. While this is a meaningful measure for a cylinder that scatters light in all directions, we cannot compute a directly equivalent grating parameter since the fields scattered by the grating are restricted to the directions of the spectral grating orders. Instead, we observe that g can be approximated by considering the scattering amplitudes in only the backward $[T_c(\pi/2)]$ and forward $[T_c(-\pi/2)]$ directions. We therefore define a new asymmetry parameter for the single cylinder

$$\tilde{g}_c = \frac{1 - \left| \frac{T_c(\pi/2)}{T_c(-\pi/2)} \right|^2}{1 + \left| \frac{T_c(\pi/2)}{T_c(-\pi/2)} \right|^2}. \tag{24}$$

The two parameters g and $\tilde{g}_c$ are compared in Fig. 7, indicating good qualitative agreement with respect to the forward scattering peaks and the shape of the curves. We note that significant discrepancies between g and $\tilde{g}_c$ occur when there is significant scattering into the backward half-plane $(0<\theta<\pi)$ but $T_c(\pi/2)\approx 0$. This effect can be seen towards the high-frequency end of Fig. 7, where $g\to 0$ but $\tilde{g}_c\approx 0.65$, however, it becomes less significant at lower frequencies when the monopole and dipole scattering terms dominate. In the dipole approximation, which was shown in Sec. III to be valid for frequencies up to the second band of the PC, the ratio of scattering amplitudes (8) in Eq. (24) can be simplified by writing $T_c(\pi/2)=b_0+2b_1$ and $T_c(-\pi/2)=b_0-2b_1$, which yields

$$\frac{T_c(\pi/2)}{T_c(-\pi/2)} = \frac{-1 + i(M_1 - 2M_0)}{3 + i(M_1 + 2M_0)}. \tag{25}$$

Since the M_n terms (5) are real, it is clear that the right-hand side of Eq. (25) can never vanish. Thus, even when there is strong forward scattering, as in Fig. 5(g), there remains a small, but finite, backscattered field and $\tilde{g}_c<1$. Recall, however, that the grating transmittance spectrum in Fig. 6 exhibits an almost zero reflectance at approximately the same frequency. To understand why the additional cylinders in the grating can lead to a null reflectance, we consider the grating equivalent of Eq. (24) which is given by

$$\tilde{g}_G = \frac{1 - \left| \frac{T_G(\pi/2)}{T_G(-\pi/2)} \right|^2}{1 + \left| \frac{T_G(\pi/2)}{T_G(-\pi/2)} \right|^2}, \tag{26}$$

where $T_G(\pi/2)=r_0$ and $T_G(-\pi/2)=t_0-1$ are the amplitudes of the scattered field components only. We note that in contrast to the single cylinder, $\tilde{g}_G=1$ corresponds to perfect transmission since, in the single grating order regime, light can be scattered in only two directions; forward or backward. Figure 7 shows $\tilde{g}_G$ plotted on the same axis as g and $\tilde{g}_c$ for the same cylinder parameters. While the $\tilde{g}_c$ and $\tilde{g}_G$ curves have significantly different shapes, the locations of the forward scattering peaks are quite similar, with excellent agreement between all three curves close to the second peak at $d/\lambda\approx 0.6$. These results demonstrate that forward scattering by each cylinder in a grating manifests as forward scattering by the grating, and hence, high transmission into the spectral grating order. As an aside, we note that the sharp feature at $d/\lambda\approx 0.55$ in the $\tilde{g}_G$ curve and also in the grating transmission spectrum in Fig. 6 resembles the resonant reflection and transmission features observed by Gantzounis *et al.* in 2D arrays of spheres [15]. While it is beyond the scope of this paper to investigate the relationship in detail, it is likely that these features have a common physical origin associated with the periodic grating structure rather than a single cylinder scattering property. Hence, it is likely that they cannot be described accurately by the single-cylinder analysis presented here.

To allow a direct mathematical comparison between the grating and cylinder scattering, we derive an equivalent expression to Eq. (25) for the ratio of the grating scattering amplitudes. In the dipole approximation

$$\frac{T_G(\pi/2)}{T_G(-\pi/2)} = \frac{b_0 + 2b_1}{b_0 - 2b_1} = \frac{(S_2' - S_0') + i(M_1 - 2M_0)}{(3S_0' + S_2') + i(M_1 + 2M_0)}, \tag{27}$$

which follows from Eqs. (21) and (22), as described in Appendix B. While there are similarities between the cylinder (25) and grating (27) forms, particularly in the imaginary part, there are also subtle, yet significant differences introduced by the addition of an array of periodically phased cylinders, the manifestation of which lies in the lattice sums, S_m'.

Explicit forms for the lattice sums have been derived by Twersky [20] and by Nicorovici *et al.* [21], and we have, in general

$$S_{2l}' = S_{2l}'^{J} + iS_{2l}'^{Y}, \tag{28}$$

$$S_{2l-1}' = iS_{2l-1}'^{J} - S_{2l-1}'^{Y}, \tag{29}$$

where

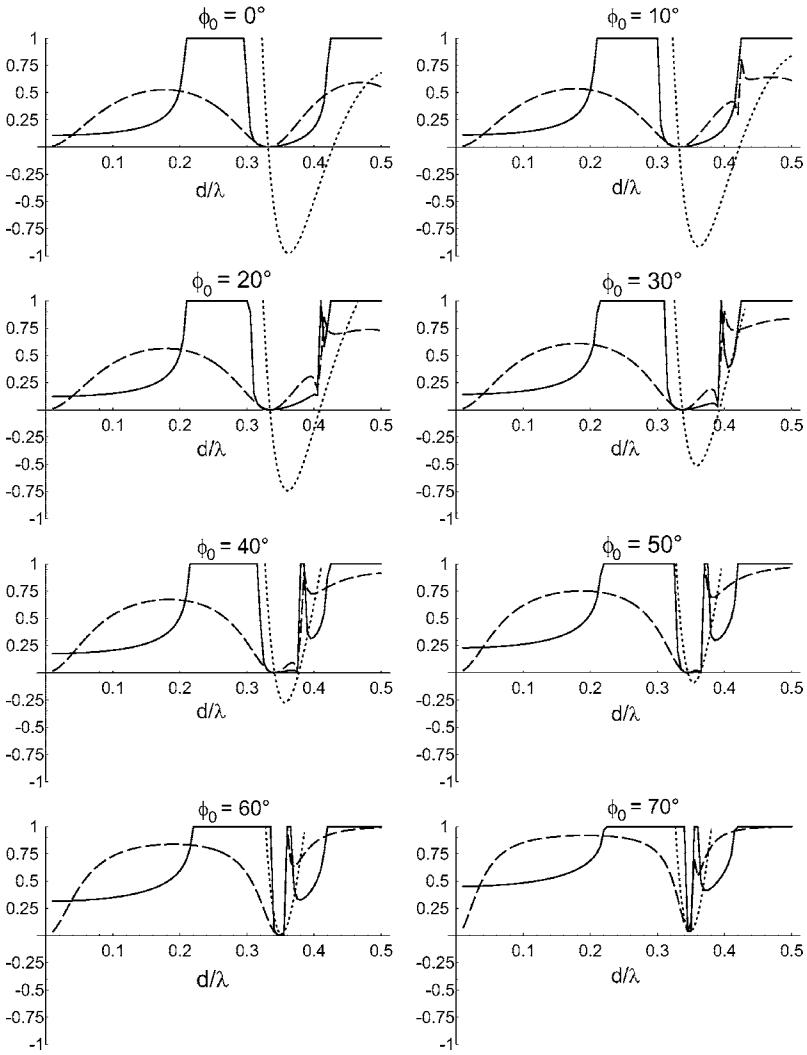

FIG. 8. Plot of the numerator of the backscattering amplitude, $T_G(\pi/2-\phi_0)$, defined in Appendix B (dotted), the reflectance of a single grating (dashed) and the semi-infinite PC (solid) as a function of normalized frequency d/λ for $\phi_0=0°-70°$ in 10° increments. Calculations are to dipole order accuracy.

$$S'^{J}_{2l} = \frac{2}{d}\sum_{p\in\Omega_p}\frac{\cos(2l\phi_p)}{\chi_p}, \tag{30}$$

$$S'^{J}_{2l-1} = \frac{2}{d}\sum_{p\in\Omega_p}\frac{\sin[(2l-1)\phi_p]}{\chi_p} \tag{31}$$

with Ω_p denoting the set of propagating plane wave orders with propagation angles ϕ_p and where the quantities S'^{Y}_{2l} and S'^{Y}_{2l} are real. In the case of normal incidence and a single propagating order, it is evident that $S'^{J}_0=S'^{J}_2=2/(\chi_0 d)=2/(kd)$ and thus Eq. (27) may be further simplified

$$\frac{T_G(\pi/2)}{T_G(-\pi/2)} = \frac{i(S'^{Y}_2 - S'^{Y}_0 + M_1 - 2M_0)}{(3S'_0 + S'_2) + i(M_1 + 2M_0)}. \tag{32}$$

What distinguishes Eq. (32) from Eq. (27) is that the numerator is now purely imaginary (rather than being complex). Thus a zero of $r_0 \propto T_G(\pi/2)$, corresponding to $\tilde{g}_G=1$, may be more easily realized through the solution of one equation, rather than through the more delicate situation in which the simultaneous solution of two equations is required. It is clear from Fig. 8(a) that such a zero can be realized and that it exactly predicts the location of the null reflectance of the grating, and in turn the semi-infinite crystal.

The procedure can be generalized to the case of off-normal incidence, provided that only a single order is propagating. For an incident angle of ϕ_0, the backward scattering amplitude is defined as $T_G(\pi/2+\phi_0)$ and the forward scattering amplitude is $T_G(-\pi/2+\phi_0)$, where the general form of these two expressions is shown in Appendix B. Although the details of the analysis are substantially more complicated, nevertheless, to the same dipole order accuracy, one can show that the numerator of $T_G(\pi/2+\phi_0)/T_G(-\pi/2+\phi_0)$ can again be rendered either purely real or purely imaginary, thus admitting the possibility of a genuine null reflectance. This is illustrated in Figs. 8(b)–8(h) for a range of angles of incidence, from which it is apparent that the reflection null is remarkably insensitive to the incidence direction. The dipole order approximation involves five quantities—three lattice sums S'_0, S'_1, and S'_2, all of which are only slow functions of the angle of incidence and frequency, and the boundary condition terms M_0 and M_1. Figure 5(d) shows that b_1 passes through a resonance close to the reflection null, and hence, it is clear that M_1 is the critical term, with its rapid change dominating the calculation and rendering the location of the

reflection null largely insensitive to the angle of incidence, and close to the single cylinder resonance.

Our procedure for computing a rational function for the back scattering ratio $T_G(\pi/2)/T_G(-\pi/2)$ (in the long wavelength limit) can be extended to quadrupole accuracy and a systematic procedure for simplifying the resultant expressions can be derived, again showing that the numerator of $T_G(\pi/2)$ can again be rendered real. While we have not proceeded beyond quadrupole order accuracy, the structure of the scattering matrix $\boldsymbol{S}'+i\boldsymbol{M}$, and the explicit form of the higher order lattice sums that are involved, lead us to conjecture that numerator of $T_G(\pi/2)$ can be made effectively real for all multipole truncation orders (in the long wavelength limit). Again, this would lead to a realizable zero of the grating reflectance and a zero of the reflectance of the semi-infinite crystal.

In the case of shorter wavelengths, however, for which there can be more than one propagating order, it is not possible to simplify the form of $T_G(\pi/2)$ so that it has a numerator that is effectively real, even for the simplest, most highly symmetric cases. The need to solve two independent simultaneous equations to locate a zero of $T_G(\pi/2)$ is much more complicated and from our computational studies, we believe that there is no zero that can be deduced for real incidence parameters. Accordingly, the near-perfect transmission into a photonic crystal thus appears limited to the case of long wavelengths (i.e., single propagating orders in reflection and transmission). As we discuss in the next section, this result has significant implications for coupling to hole-type PCs.

VI. DISCUSSION

Our analysis in Secs. IV and V gives a rigorous justification for the numerical observations discussed in Secs. II and III for coupling to rod-type PCs. While we have presented results for purely two-dimensional structures, the conclusions are also applicable to three-dimensional PC slab geometries in which highly efficient, wide-angle coupling has been demonstrated numerically [9]. The results show that almost perfect coupling coincides with nulls in the reflection spectrum of a single grating layer of the PC, which in turn are located close to the forward scattering resonances of the individual cylinders. Although the analysis presented here is valid only in the long-wavelength regime where there is a single propagating grating order, the conditions for perfect grating transmission are unlikely to occur at higher frequencies for reasons described in Sec. V. Furthermore, a minimum frequency condition is imposed by the requirement for significant dipole or higher order scattering by each cylinder to ensure strong forward scattering, as discussed in Sec. III. These two conditions provide an intuitive explanation for why rod-type PCs typically exhibit highly efficient coupling over a wide range of incident angles, whereas air-hole PCs may require interface modifications in order to achieve satisfactory results [5,7,6].

For rod-type PCs, where the background refractive index is lower than that of the rods, the single grating order regime typically extends to frequencies above the second or third pass band as shown in Fig. 2, and thus there is a wide parameter space in which to satisfy the forward scattering condition for the individual cylinders. In air hole PC structures it is much more difficult to satisfy both conditions simultaneously since nonisotropic scattering from air holes only occurs at relatively high frequencies but at the same time the high index background reduces the frequency at which multiple plane wave orders appear. For example, if the background material is silicon ($\nu=3.4$), the first nonzero grating order appears for large angles of incidence at frequencies above $d/\lambda=0.15$, which is well below the second band for most air-hole PCs.

In conclusion, we have demonstrated highly efficient, wide angle coupling to uniform rod-type PCs without modification to the interface. Almost perfect coupling occurs for a wide range of rod-type PC structures and for both TE and TM polarizations when the grating layers that form the PC transmit all incident light into a single diffracted order. Using a combination of semianalytic and numerical analysis, we have shown that such behavior is closely related to the forward scattering resonances of each constituent cylinder, and thus depends only weakly on the incident angle and grating period. Finally, we have identified the conditions that must be satisfied in order to achieve highly efficient coupling in rod-type PCs. PC structures designed to operate under these conditions could enhance significantly the efficiency of in-band PC devices.

ACKNOWLEDGMENT

This work was produced with the assistance of the Australian Research Council under the ARC Centres of Excellence program.

APPENDIX A: DERIVATION OF GRATING REFLECTION AND TRANSMISSION AMPLITUDES

Following from Eq. (21), the reflected and transmitted plane wave coefficients may be reconstructed using Green's theorem and the Cartesian form of the Green's function to derive [17]

$$\boldsymbol{r}=\frac{2}{d}\boldsymbol{\chi}^{-1/2}\boldsymbol{K}^{+}\boldsymbol{b}, \tag{A1}$$

$$\boldsymbol{t}=\boldsymbol{\delta}+\frac{2}{d}\boldsymbol{\chi}^{-1/2}\boldsymbol{K}^{-}\boldsymbol{b}, \tag{A2}$$

where $\boldsymbol{K}^{+}=[K^{+}_{pn}]$, with $K^{+}_{np}=\exp(-in\phi_p)$, and $\boldsymbol{K}^{-}=[K^{-}_{pn}]$, with $K^{-}_{np}=(-1)^n\exp(in\phi_p)$. At frequencies where only a single plane wave order propagates, these two expressions reduce to Eqs. (22) and (23).

APPENDIX B: DERIVATION OF GRATING SCATTERING FUNCTIONS $T_G(\pi/2)$ AND $T_G(-\pi/2)$

The derivation of the reflected field, $T_G(-\pi/2)=r_0$ follows from Eqs. (21), (A1), and (22). In the dipole approximation we can write

$$T_G(\pi/2) = b_{-1} + b_0 + b_1 = b_0 + 2b_1,$$

$$= \boldsymbol{K}^+(\boldsymbol{S}' + I\boldsymbol{M})^{-1}\boldsymbol{J}^-,$$

$$= (1\ 1\ 1)\begin{pmatrix} S_0' + iM_1 & 0 & S_2' \\ 0 & S_0' + iM_0 & 0 \\ S_2' & 0 & S_0' + iM_1 \end{pmatrix}^{-1}\begin{pmatrix} -1 \\ 1 \\ -1 \end{pmatrix},$$

$$= \frac{(S_2' - S_0') + i(M_1 - 2M_0)}{(S_0' + iM_1)(S_0' + S_2' + iM_1)}, \tag{B1}$$

where, in simplifying the expressions, we have made use of the lattice sum identities $S'_{-l} = (-1)^l S'_l$ and, in the case of normal incidence $S'_{2l-1} = 0$. Similarly, the component of the field scattered in the forward direction is given by

$$T_G(-\pi/2) = t_0 - 1,$$

$$= -b_{-1} + b_0 - b_1 = b_0 - 2b_1,$$

$$= \frac{(3S_0' + S_2') + i(M_1 + 2M_0)}{(S_0' + iM_1)(S_0' + S_2' + iM_1)}. \tag{B2}$$

Equation (27) follows directly from the ratio of Eqs. (B1) and (B2).

In the general case for non-normal incidence at an angle ϕ_0, the backward scattering amplitude in the dipole approximation is given by

$$T_G(\pi/2 + \phi_0)$$

$$= \boldsymbol{K}^+(\boldsymbol{S}' + I\boldsymbol{M})^{-1}\boldsymbol{J}^-$$

$$= (e^{i\phi_0}\ 1\ e^{-i\phi_0})$$

$$\times \begin{pmatrix} S_0' + iM_1 & -S_1' & S_2' \\ S_1' & S_0' + iM_0 & -S_1' \\ S_2' & S_1' & S_0' + iM_1 \end{pmatrix}^{-1}\begin{pmatrix} -e^{i\phi_0} \\ 1 \\ -e^{-i\phi_0} \end{pmatrix}, \tag{B3}$$

and a similar expression can be found for the forward scattering amplitude $T_G[-(\pi/2 + \phi_0)]$.

[1] A. Mekis and J. D. Joannopoulos, J. Lightwave Technol. **19**, 861 (2001).
[2] W. Kuang, C. Kim, A. Stapleton, and J. D. O'Brien, Opt. Lett. **27**, 1604 (2002).
[3] A. Talneau, P. Lalanne, M. Agio, and C. M. Soukoulis, Opt. Lett. **27**, 1522 (2002).
[4] P. E. Barclay, K. Srinivasan, M. Borselli, and O. Painter, Appl. Phys. Lett. **85**, 4 (2004).
[5] T. Baba and D. Ohsaki, Jpn. J. Appl. Phys., Part 1 **40**, 5920 (2001).
[6] J. Witzens, M. Hochberg, T. Baehr-Jones, and A. Scherer, Phys. Rev. E **69**, 046609 (2004).
[7] B. Momeni and A. Adibi, Appl. Phys. Lett. **87**, 171104 (2005).
[8] J. Witzens and A. Scherer, J. Opt. Soc. Am. A **20**, 935 (2003).
[9] T. P. White, C. M. de Sterke, R. C. McPhedran, and L. C. Botten, Appl. Phys. Lett. **87**, 111107 (2005).
[10] L. C. Botten, T. P. White, A. A. Asatryan, T. N. Langtry, C. Martijn de Sterke, and R. C. McPhedran, Phys. Rev. E **70**, 056606 (2004).
[11] T. P. White, L. C. Botten, C. Martijn de Sterke, R. C. McPhedran, A. A. Asatryan, and T. N. Langtry, Phys. Rev. E **70**, 056607 (2004).
[12] E. N. Economou and A. Zdetsis, Phys. Rev. B **40**, R1334 (1989).
[13] *Photonic Bandgaps and Localization*, edited by C. M. Soukoulis (Plenum Press, New York, 1993).
[14] E. Lidorikis, M. M. Sigalas, E. N. Economou, and C. M. Soukoulis, Phys. Rev. Lett. **81**, 1405 (1998).
[15] G. Gantzounis and N. Stefanou, Phys. Rev. B **72**, 075107 (2005).
[16] H. C. van de Hulst, *Light Scattering by Small Particles* (Wiley, New York, 1957).
[17] L. C. Botten, N. A. Nicorovici, A. A. Asatryan, R. C. McPhedran, C. M. de Sterke, and P. A. Robinson, J. Opt. Soc. Am. A **17**, 2165 (2000).
[18] *Handbook of Mathematical Functions*, 9th ed., edited by M. Abramowitz and I. A. Stegun (Dover, New York, 1970).
[19] L. C. Botten, N. A. Nicorovici, R. C. McPhedran, C. Martijn de Sterke, and A. A. Asatryan, Phys. Rev. E **64**, 046603 (2001).
[20] V. Twersky, Arch. Ration. Mech. Anal. **8**, 323 (1961).
[21] N. A. Nicorovici and R. C. McPhedran, Phys. Rev. E **50**, 3143 (1994).